

Some spectral properties of the quasar ultraviolet bump

O. Torbaniuk

Taras Shevchenko National University of Kyiv, Faculty of Physics, Kyiv, Ukraine.

G. Ivashchenko

Taras Shevchenko National University of Kyiv, Astronomical Observatory, Kyiv, Ukraine.

O. Sergijenko

Ivan Franko National University of Lviv, Astronomical Observatory, Lviv, Ukraine.

Abstract. In the present work the part of the quasar UV-optical bump within the wavelength range 1210 – 1450 Å was studied with the help of composite spectra compiled from the samples of SDSS DR7 spectra with the similar spectral index α_λ within 1270 – 1480 Å. This division allowed to see weak emission lines, which were not detected in previous studies of the quasar composite spectra, but were known from individual optical or composite UV spectra from the Hubble Space Telescope. Although the physical explanation of the difference in spectral indices between quasars and their dependence on quasar parameters is still not clear, it is obvious that this difference has to be taken into account when generating composite spectra, e.g. for redshift measurements. It was also shown that the equivalent width of the emission lines does not depend on the spectral index.

Introduction

The spectral energy distribution of quasars in UV-optical range is characterised by the so called Big Blue Bump with a pick around $\lambda_{rest} = 1000 - 1300 \text{ \AA}$, broad emission lines of hydrogen Lyman and Balmer series and low-ionized metals (e.g. CIV, SiIII, MgII etc.), broad absorption lines (only in $\sim 10\%$ of quasars) and decrement of the flux blueward of 1215 Å due to absorption by intergalactic H I (the Ly α forest). It is believed that the (mostly thermal) continuum and emission lines originate from the hot accretion disk and circumnuclear fast moving clumps of gas, correspondingly. The proximity of these regions is considered to be the most promising explanation of the Baldwin effect [Baldwin, 1977]: the inverse correlation of equivalent width of some emission lines with the monochromatic fluxes at UV region (in most cases the flux at 1450 Å or 2500 Å is considered in the literature [e.g. Dietrich et al., 2002; Wu et al., 2009]).

Due to remarkable similarity of the quasar spectra from object to object, the mean, or composite, spectra are usually used to study the general spectral properties of quasars. They are also widely used as templates for redshift determination (mainly in automatic redshift surveys). The averaging over several hundreds or even thousands of (usually) medium-resolution spectra allows to increase the signal-to-noise ratio and to reveal tiny features unseen in individual spectra. The composite spectra of quasars in ultraviolet-optical band were compiled for a wide set of quasar samples [Brotherton et al., 2001; Francis et al., 1991; Scott et al., 2004; Vanden Berk et al., 2001]. They also used in Ly α -forest studies [e.g. Bernardi et al., 2003; Desjacques et al., 2007; Polinovskyi and Malygin, 2010]. One of the main sources of uncertainties during the generation of the quasar composite spectra is the difference in spectral shape of individual objects (despite of the general similarity), e.g. the difference in spectral index α_λ of the red part of UV- optical bump. Thus in the present work to study the part of the UV-optical bump we used the composite spectra compiled by us from samples of spectra with similar α_λ .

The data

For our study we used 16 composite spectra of quasars compiled by us [Ivashchenko et al., 2012]. Each of these spectra was generated of 200 individual ones with similar spectral indices α_λ within the range 1270 – 1480 Å namely from those that have the values of α_λ close to $-0.6 - k \cdot 0.1$, where $k = 1..16$ is the composite number. These subsamples were taken from the publicly available release of the sky-residual subtracted spectra [Wild and Hewett, 2010] for the Sloan Digital Sky Survey (SDSS) Legacy

Release 7 [Abazajian et al., 2009]. The spectral indices for individual spectra were calculated considering the continuum of the quasar spectra redward of the Ly α emission line (1215 Å) to be a power-law $\sim \lambda^{\alpha_\lambda}$, and using the following wavelength ranges, which are the most free from emission lines: 1278–1286, 1320–1326, 1345–1360 and 1440–1480 Å. The mean arithmetic spectra were obtained after (i) division of each individual spectrum on its normalization constant (the mean flux over all pixels within the rest wavelength range 1450–1470 Å), (ii) rebinning them with $\Delta\lambda_{rest} = 2 \text{ \AA}$, and (iii) stacking the spectra into the rest frame. The dispersion σ^2 of each pixel of the composite spectrum is calculated from the noises σ_i of pixels of individual spectra as $\sigma^{-2} = \sum_i \sigma_i^{-2}$.

The spectral indices of the composite spectra were calculated in the way mentioned above, but the parts of the spectra which are the most free from emission lines were selected manually in each composite. The parts of spectra used for calculating the spectral index are shown in Figure 1 (*short-dashed* line, the highest spectra are the steepest ones). Three spectra with the slopes -0.84 , -1.49 and -2.12 are shown with the *solid* lines together with the fitted power-law continua (*dashed* lines). The regions used for continuum fitting slightly vary from spectrum to spectrum which is probably caused by changing of intensity of weak emission lines. It is worth to note that there is no absolutely emission line-free region in UV-optical bump, and selection of lines-free regions means selection of regions with the weakest emission lines.

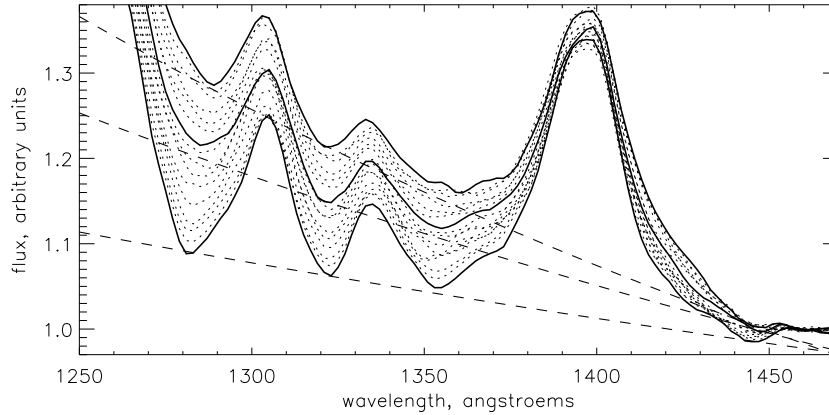


Figure 1. The parts of the composite spectra used for continuum approximation. See explanation in the text.

Table 1. The mean redshift \bar{z} , spectral index α_λ , and the mean monochromatic luminosity $\langle \log l_{1450} \rangle$ at 1450 Å for 16 composites.

| n | α_λ | \bar{z} | $\langle \log l_{1450} \rangle$ |
|----|------------------|-----------------|---------------------------------|
| 1 | -0.84 ± 0.04 | 2.90 ± 0.54 | 42.70 ± 0.21 |
| 2 | -0.92 ± 0.03 | 2.89 ± 0.53 | 42.72 ± 0.21 |
| 3 | -0.99 ± 0.02 | 2.87 ± 0.51 | 42.72 ± 0.21 |
| 4 | -1.02 ± 0.05 | 2.85 ± 0.49 | 42.72 ± 0.24 |
| 5 | -1.19 ± 0.02 | 2.82 ± 0.43 | 42.73 ± 0.24 |
| 6 | -1.30 ± 0.02 | 2.84 ± 0.49 | 42.74 ± 0.21 |
| 7 | -1.42 ± 0.03 | 2.82 ± 0.44 | 42.76 ± 0.23 |
| 8 | -1.42 ± 0.02 | 2.76 ± 0.40 | 42.78 ± 0.21 |
| 9 | -1.49 ± 0.05 | 2.77 ± 0.44 | 42.78 ± 0.25 |
| 10 | -1.55 ± 0.03 | 2.80 ± 0.46 | 42.79 ± 0.27 |
| 11 | -1.67 ± 0.01 | 2.75 ± 0.45 | 42.78 ± 0.25 |
| 12 | -1.83 ± 0.04 | 2.75 ± 0.43 | 42.78 ± 0.22 |
| 13 | -1.86 ± 0.04 | 2.74 ± 0.43 | 42.77 ± 0.24 |
| 14 | -1.99 ± 0.03 | 2.72 ± 0.42 | 42.74 ± 0.23 |
| 15 | -2.00 ± 0.02 | 2.74 ± 0.42 | 42.74 ± 0.23 |
| 16 | -2.12 ± 0.03 | 2.74 ± 0.43 | 42.75 ± 0.24 |

The spectral indices for the composite spectra, the mean redshift of the corresponding sample, and

the mean logarithm of the quasar monochromatic luminosity at 1450 Å, $\langle \log l_{1450} \rangle$, are presented in Table 1. The value $\log l_{1450}$ for individual spectra was calculated using the mean flux within the wavelength range 1449 – 1451 Å and photometric distance to the quasar obtained within the spatially flat Λ CDM cosmological model with the matter density parameter $\Omega_M = 0.27$ and Hubble constant $H_0 = 70.5 \text{ km s}^{-1} \text{ Mpc}^{-1}$. The quoted error bars are the root mean squares for the corresponding distributions for z and $\langle \log l_{1450} \rangle$, and 1σ errors for α_λ , correspondingly.

The method

The wavelength ranges (a) 1215–1321 Å and (b) 1323–1447 Å (Figure 2) were considered separately and fitted with a superposition of continuum and the smallest possible number of emission lines in the form:

$$f(\lambda^{rest}) = C + \sum_i a_i \exp \left[-\frac{(\lambda^{rest} - \lambda_i^0)^2}{2w_i^2} \right], \quad (1)$$

where in case (a) $C = b$, i. e. the continuum is fitted with a constant, and in case (b) $C = d\lambda^{\alpha_\lambda}$ with fixed α_λ from Table 1. The values of b , d , a_i , w_i , λ_i^0 were calculated in the following two steps: (i) using the IDL `lmfit` subroutine for each multiplet the best fit model (based on the minimal $\chi^2/\text{d.o.f.}$) in a form of (1) was found; (ii) the central wavelengths λ^0 obtained at the first step were fixed and the best fit values of other parameters $\{b, d, a_k, w_k\}$ with the 1σ errors from the extremal values of the N-dimensional distribution were calculated by the Markov Chain Monte Carlo (MCMC) method using `CosmoMC` package [Lewis and Bridle, 2002] as a generic sampler (with the values of $\{b, d, a_k, w_k\}$ obtained at the first step as starting values). The MCMC technique has been chosen as it is a fast and accurate method of exploration of high-dimensional parameter spaces. In each case we generated 8 chains which have converged to $R-1 < 0.0075$. Due to the small values of the flux dispersion σ_f^2 in composite spectra determined from the covariance matrix to estimate errors correctly we introduced the additional intrinsic errors σ_{int} such that the total dispersion, $\sigma^2 = \sigma_f^2 + \sigma_{int}^2$, results in the minimal $\chi^2/\text{d.o.f.}$ to be $1 - 0$.

For separate lines or sum of lines the equivalent widths were calculated. In each case the area under the lines was calculated as an integral of an analytic function (Gaussian or several Gaussians) with the obtained parameters.

Results and discussion

In Figure 3 one of composite spectra with $\alpha_\lambda = -0.92$ is shown with the best fits for both regions as an example. The dashed lines indicate the emission lines found in spectrum. The labels X_1 – X_5 stand for components, identification of which was not found in the literature. In Table 2 the central wavelengths of emission lines from all 16 spectra are presented along with possible identification and corresponding laboratory rest wavelengths. The obtained parameters for each line (amplitude and FWHM) will be presented elsewhere. The identification of lines was made using known emission lines from the literature. The following lines were found by Vanden Berk et al. [2001] in composite spectrum of 2200 quasars from SDSS without taking into account any differences in spectra shape: Ly α +OIV (one feature), NV, SiII, OI+SiIII (one feature), CII and SiIV+OIV] (one feature). The separate components of these emission features as far as other lines found in the present work are known from works on ultraviolet individual [Laor et al., 1994, 1995, 1997] and composite [Brotherton et al., 1994] spectra of quasars from the Hubble Space Telescope, and from empirical UV template for Fe emission in quasars obtained by Vestergaard and Wilkes [2001] from the galaxy I Zwicky 1. All the lines, for which we did not find any possible candidates in the literature could be new lines, not noticed by other authors due to their small intensity, as well as additional components of the known lines originated due to some special physical conditions in the broad line regions in a quasar.

In Figure 4 the spectral index – equivalent width (for separate lines or sum of lines) diagrams are presented. We applied the F-test and found that for all emission features presented in this figure the values of equivalent width do not depend on the spectral index. This result is an expected one if we take into account the Baldwin effect and the absence of luminosity-dependence of the spectral index, as it is seen from Table 1. On the other hand, the mean redshift of the subsamples slightly increases with α_λ , that could be an evidence for evolution of α_λ with time, but also can be caused by some selection effects. Although the physical explanation of the difference in spectral indices between quasars and their dependence on quasar parameters is still not clear, it is obvious that this difference has to be taken into account when generating the composite spectra, e. g. for redshift determination. When using composite spectra made without taking into account the difference in spectral shape one usually deals with larger

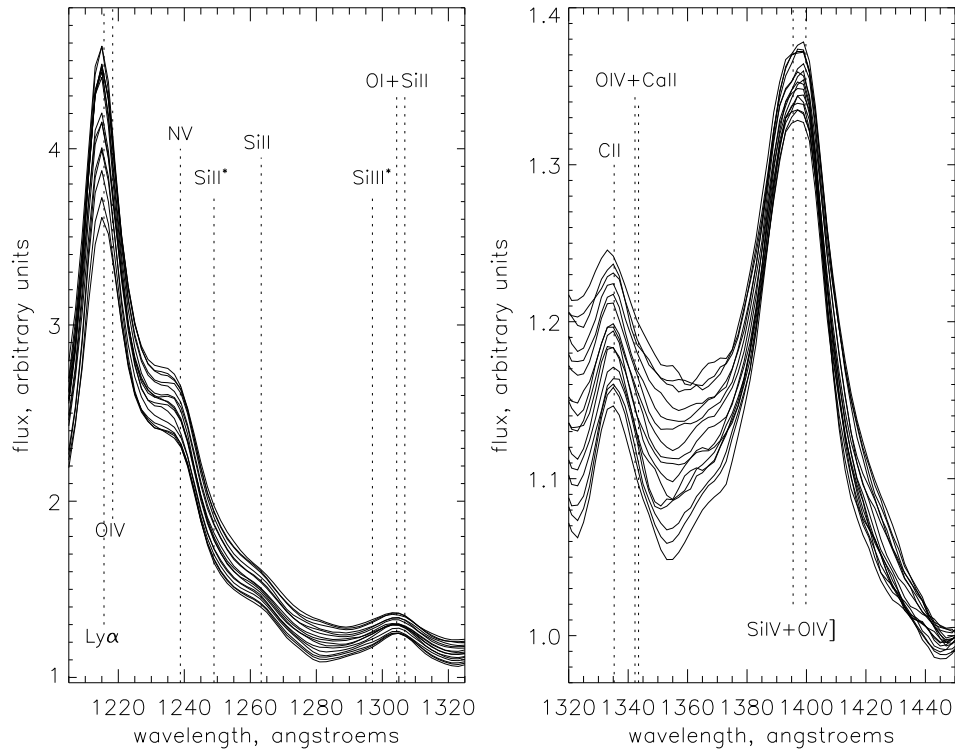


Figure 2. Wavelength ranges 1215–1320 Å (left) and 1323–1443 Å (right). Dashed lines indicate the central wavelengths of the emission lines found by Vanden Berk et al. [2001]. Here asterisk indicates more than one allowed value of the total angular momentum J for that specific term and transition, “[” means intercombination transitions.

noise and thus treats blended emission features as one line, increasing the errors in central wavelengths and, hence, in line identification.

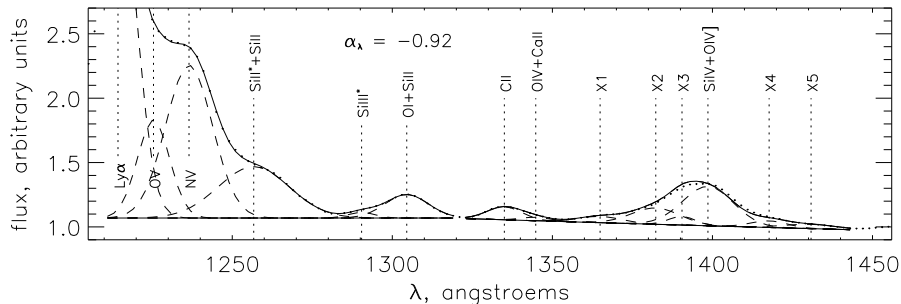


Figure 3. The composite spectrum with $\alpha_\lambda = -0.92$ with the best fits for both two regions. The dashed lines indicate the found emission lines, while short-dashed lines indicate their central wavelengths. X1 – X5 stand for lines which were not identified by us.

Acknowledgments. This work has been supported by Swiss National Science Foundation (SCOPES grant No 128040). The authors are thankful to the Sloan Digital Sky Survey team. Funding for the SDSS has been provided by the Alfred P. Sloan Foundation, the Participating Institutions, the National Aeronautics and Space Administration, the National Science Foundation, the US Department of Energy, the Japanese Monbukagakusho, and the Max Planck Society. The authors also acknowledge the usage of CosmoMC package.

References

- Abazajian, K. N. et al., The Seventh Data Release of the Sloan Digital Sky Survey, *Astrophys. J. (Supp.)*, 182, 543–558, 2009.
- Baldwin, J. A., Luminosity Indicators in the Spectra of Quasi-Stellar Objects, *Astrophys. J.*, 214, 679–684, 1977.

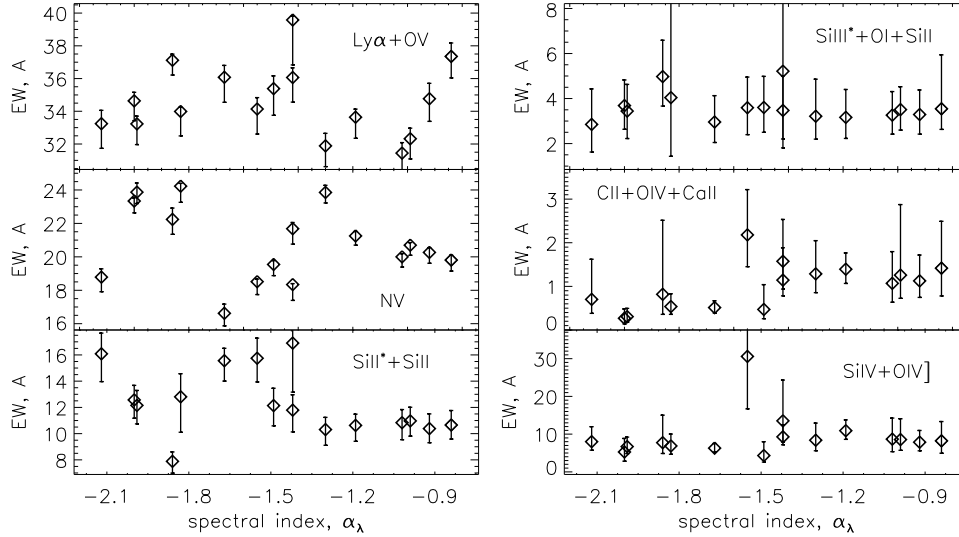


Figure 4. The spectral index – equivalent width of lines or sum of lines (in Å) diagram.

- Bernardi, M. et al., A Feature at $z \sim 3.2$ in the Evolution of the Ly α Forest Optical Depth, *Astron. J.*, , 125, 32–52, 2003.
- Brotherton, M. S., Wills, B. J., Francis, P. J., and Steidel, C. C., The intermediate line region of QSOs, *Astrophys. J.*, 430, 495–504, 1994.
- Brotherton, M. S., Tran, H. D., Becker, R. H., Gregg, M. D., Laurent-Muehleisen, S. A., and White, R. L., Composite Spectra from the FIRST Bright Quasar Survey, *Astrophys. J.*, 546, 775–781, 2001.
- Desjacques, V., Nusser, A., and Sheth, R. K., The probability distribution function of the Lyman α transmitted flux from a sample of Sloan Digital Sky Survey quasars, *Mon. Not. R. Astron. Soc.*, 374, 206–219, 2007.
- Dietrich, M. et al., Continuum and Emission-Line Strength Relations for a Large Active Galactic Nuclei Sample, *Astrophys. J.*, 581, 912–924, 2002.
- Francis, P. J., Hewett, P. C., Foltz, C. B., Chaffee, F. H., Weymann, R. J., and Morris, S. L., A high signal-to-noise ratio composite quasar spectrum, *Astrophys. J.*, 373, 465–470, 1991.
- Ivashchenko, G., Sergijenko, O., and Torbaniuk, O., Improved technique for quasar composite spectra generation, in *Proceedings of VI European Summer School on Experimental Nuclear Astrophysics*, edited by PoS, Proceedings of Science, *accepted for publication*, 2012.
- Laor, A. et al., The ultraviolet emission properties of five low-redshift active galactic nuclei at high signal-to-noise ratio and spectral resolution, *Astrophys. J.*, 420, 110–135, 1994.
- Laor, A., Bahcall, J. N., Jannuzi, B. T., Schneider, D. P., and Green, R. F., The Ultraviolet Emission Properties of 13 Quasars, *Astrophys. J. (Supp.)*, 99, 1, 1995.
- Laor, A., Jannuzi, B. T., Green, R. F., and Boroson, T. A., The Ultraviolet Properties of the Narrow-Line Quasar I ZW 1, *Astrophys. J.*, 489, 656, 1997.
- Lewis, A. and Bridle, S., Cosmological parameters from CMB and other data: A Monte Carlo approach, *Phys. Rev. D Part. Fields*, 66, 103 511, 2002.
- Polinovskyi, G. and Malygin, M., Mean Transmitted Flux in the Ly α Forest from a Sample of 2QZ Quasars, in *WDS'10 Proceedings of Contributed Papers: Part III – Physics*, pp. 163–168, 2010.
- Scott, J., Kriss, G., Brotherton, M., Green, R., Hutchings, J., Shull, J., and Zheng, W., A Composite Extreme Ultraviolet QSO Spectrum from FUSE, in *AGN Physics with the Sloan Digital Sky Survey*, edited by G. T. Richards & P. B. Hall, vol. 311 of *Astronomical Society of the Pacific Conference Series*, p. 31, 2004.
- Vanden Berk, D. E. et al., Composite Quasar Spectra from the Sloan Digital Sky Survey, *Astron. J.*, , 122 549–564, 2001.
- Vestergaard, M. and Wilkes, B. J., An Empirical Ultraviolet Template for Iron Emission in Quasars as Derived from I Zwicky 1, *Astrophys. J. (Supp.)*, 134, 1–33, 2001.

TORBANIUK ET AL.: SOME SPECTRAL PROPERTIES OF THE QUASAR UV BUMP

Wild, V. and Hewett, P. C., Peering through the OH Forest: public release of sky-residual subtracted spectra for SDSS DR7, *ArXiv e-prints*, 2010.

Wu, J., Vanden Berk, D. E., Brandt, W. N., Schneider, D. P., Gibson, R. R., and Wu, J., Probing The Origins of the C IV and Fe K α Baldwin Effects, *Astrophys. J.*, *702*, 767–778, 2009.

Table 2. The central wavelength of emission lines found in spectra. Lines in brackets are probably components of one found emission feature. X1 etc. stand for lines which were not identified by us. Here asterisk indicates more than one allowed value of the total angular momentum J for that specific term and transition, “[j]” means intercombination transitions.

| | 1 | 2 | 3 | 4 | 5 | 6 |
|-----------------|------------------|--------------------|--|---|---------------|---|
| | Ly α +OIV | NV | SiII*+SiII | SiIII*+OI+SiII | CII+OIV+CaII | SiIV+OIV]+X ₁ +... |
| λ_{lab} | 1215.7+1218.3 | 1238.8+ +1242.8 | [1248.4+1251.1]+ +[1260.4+1264.7+ +1265.0] | [1295.5+1298.9]+ +[1302.2+1304.6+ +1306.0+1309.3] | 1335.3 | 1395.5+1399.8+ +1401.8+1407.4 |
| 1 | 1214.4+1225.6 | 1236.9 | 1256.7 | 1290.4+1304.4 | 1334.5+1346.7 | 1368.2+1382.5+1390.4+1399.8+1418.7+1436.3 |
| 2 | 1214.3+1225.4 | 1236.5 | 1256.7 | 1290.4+1304.5 | 1335.0+1344.8 | 1364.9+1382.3+1390.5+1399.6+1417.7+1430.8 |
| 3 | 1214.3+1225.0 | 1236.1 | 1256.7 | 1289.7+1304.1 | 1334.9+1343.2 | 1364.4+1380.1+1390.3+1399.3+1418.7+1431.4 |
| 4 | 1214.8+1226.4 | 1236.4 | 1257.0 | 1290.6+1304.2 | 1334.7+1341.4 | 1364.8+1376.9+1386.5+1392.0+1399.0+1412.3+1419.6+1439.5 |
| 5 | 1214.3+1225.3 | 1236.0 | 1256.7 | 1291.4+1304.5 | 1335.8 | 1370.5+1396.5+1401.7+1410.9+1422.4+1436.4 |
| 6 | 1214.2+1224.3 | 1234.8 | 1256.5 | 1290.1+1304.4 | 1334.6+1348.5 | 1361.4+1382.1+1389.8+1399.3+1407.4+1435.4 |
| 7 | 1213.2+1221.6 | 1236.1 | 1253.4 | 1300.4+1305.2 | 1334.9 | 1362.6+1394.5+1396.5+1418.9 |
| 8 | 1213.8+1223.7 | 1235.9 | 1255.7 | 1285.7+1303.6 | 1334.2+1344.1 | 1363.0+1382.0+1390.3+1399.6+1413.3+1430.7+1438.6 |
| 9 | 1213.4+1223.4 | 1236.3 | 1255.6 | 1286.6+1303.6 | 1334.1+1343.2 | 1378.0+1394.0+1400.2+1405.8+1415.7+1425.6+1438.3 |
| 10 | 1213.8+1223.9 | 1235.5 | 1252.7 | 1288.6+1304.6 | 1332.1 | 1372.3+1395.4+1400.6+1407.9+1418.5+1428.4 |
| 11 | 1213.7+1223.4 | 1236.2 | 1252.3 | 1288.4+1304.0 | 1334.0+1342.3 | 1376.2+1395.6+1401.5+1408.7+1421.0+1436.6 |
| 12 | 1214.5+1225.7 | 1235.1 | 1256.0 | 1281.9+1301.6+1304.9 | 1334.8+1345.1 | 1385.1+1393.9+1401.0+1407.8+1423.3+1438.5 |
| 13 | 1214.5+1225.8 | 1237.4 | 1250.8+1258.4 | 1276.7+1304.5 | 1333.9+1336.0 | 1376.0+1397.9+1419.3+1429.8 |
| 14 | 1214.4+1225.0 | 1235.1 | 1255.7 | 1286.2+1304.0 | 1335.3 | 1388.8+1398.5+1422.1 |
| 15 | 1213.7+1223.2 | 1235.5 | 1256.1 | 1283.7+1303.2 | 1335.8 | 1396.8+1397.3 |
| 16 | 1214.1+1224.1 | 1235.6 | 1252.4 | 1285.6+1302.2 | 1333.7+1343.7 | 1371.8+1397.4+1416.8+1425.7 |